

Global phase diagram of two-dimensional dirty hyperbolic Dirac liquids

Christopher A. Leong,¹ Daniel J. Salib,¹ and Bitan Roy¹

¹*Department of Physics, Lehigh University, Bethlehem, Pennsylvania, 18015, USA*

(Dated: December 5, 2025)

Within the framework of the canonical nearest-neighbor tight-binding model for spinless fermions, a family of two-dimensional bipartite hyperbolic lattices hosts massless Diraclike excitations near half-filling with the iconic vanishing density of states (DOS) near zero energy. We show that a collection of such ballistic quasiparticles remains stable against sufficiently weak pointlike charge impurities, a feature captured by the vanishing average $[\rho_a(0)]$ and typical $[\rho_t(0)]$ DOS at zero energy, computed by employing the kernel polynomial method in sufficiently large $\{10, 3\}$ hyperbolic lattices (Schläfli symbol) with more than 10^8 and 10^5 sites, respectively, with open boundary conditions. However, at moderate disorder the system enters a metallic state via a continuous quantum phase transition where both $\rho_a(0)$ and $\rho_t(0)$ become finite. With increasing strength of disorder, ultimately an Anderson insulator sets in, where only $\rho_t(0) \rightarrow 0$. The resulting phase diagram for dirty Dirac fermions living on a hyperbolic space solely stems from the background negative spatial curvature, as confirmed from the vanishing $\rho_t(0)$ for arbitrarily weak disorder on honeycomb lattices, fostering relativistic fermions on a flatland, as the thermodynamic limit is approached.

Introduction. The nearest-neighbor (NN) tight binding model (TBM), simple yet succinctly captures a plethora of robust emergent phenomena in a number of quantum crystals, harboring noninteracting free fermions [1]. Notably, interesting phenomena stem from this model, when employed on a family of two-dimensional (2D) bipartite hyperbolic lattices [2, 3]. Owing to infinitely many possible realizations, 2D hyperbolic lattices, generated from periodic tiling of regular polygons with p arms (p -gons) on a curved 2D space with a constant negative curvature, each vertex of which has a coordination number of q , are characterized by the Schläfli symbol $\{p, q\}$. Together, p and q satisfy the inequality $(p-2)(q-2) > 4$, sourcing many peculiarities [4–13]. The NN-TBM on hyperbolic lattices with $p/2$ as an odd integer and $q = 3$ yields emergent massless Dirac fermions at half filling, living on a negatively curved space featuring the hallmark vanishing density of states (DOS) near zero energy [2, 3]. A Euclidean counterpart of such an emergent phenomenon is observed on a half-filled honeycomb lattice, resulting from the solution of $(p-2)(q-2) = 4$ with $p = 2q = 6$. The NN-TBM therein yields massless Dirac fermions on a relativistic flatland with the characteristic linearly vanishing DOS near zero energy [14, 15]. Therefore, $\{4n+2, 3\}$ hyperbolic lattices with integer $n > 1$ offer a unique opportunity to witness the nontrivial signatures of constant negative curvature on the quantum properties of relativistic fermions.

In this work, we numerically scrutinize the stability of lattice-regularized hyperbolic Dirac fluids in the presence of random pointlike charge impurities. Somewhat surprisingly (reasoned shortly), we find that the quantum fluid of such ballistic relativistic quasiparticles is stable against sufficiently weak disorder, identified from the *vanishing* average and typical DOS at zero energy, denoted by $\rho_a(0)$ and $\rho_t(0)$, respectively. At moderate disorder, the system enters into a diffusive metallic

state via a quantum phase transition (QPT) where both $\rho_a(0)$ and $\rho_t(0)$ become *finite*. As the disorder strength is increased further a second QPT triggers a metal-to-insulator Anderson QPT across which only $\rho_t(0) \rightarrow 0$. We arrive at these conclusions by computing the average and typical DOS with varying disorder strength (W) in sufficiently large $\{10, 3\}$ hyperbolic lattices with open boundary conditions, containing more than 10^8 and 10^5 sites, respectively, employing the kernel polynomial method (KPM) [16]. The results are shown in Fig. 1.

To unfold the unconventionality of our findings, it is worth mentioning that a stable disordered semimetal with a vanishing DOS and a disorder-driven semimetal-to-metal QPT, leading to the formation of a stable metallic phase in a 2D electronic fluid belonging to the (chiral) orthogonal symmetry class, go against the traditional wisdom [17, 18]. We contrast these results with the ones on dirty honeycomb lattices, where $\rho_t(0) \rightarrow 0$ for arbitrarily weak disorder as the thermodynamic limit is approached, confirming the presence of only an Anderson insulator therein. Thus, our findings should solely be attributed to the background negative curvature of the planar hyperbolic space, harboring gapless Dirac fermions.

The Anderson metal-to-insulator transition in a planar orthogonal class system is also unusual. Nonetheless, such a transition has previously been reported [19] and justified [20], however, only in hyperbolic Fermi liquids, displaying a *finite* $\rho_a(0)$ in clean systems, as realized in $\{8, 3\}$ and $\{8, 8\}$ lattices. However, the Anderson metal-to-insulator transition in hyperbolic Dirac systems remained unnoticed so far. Our findings, in this context, therefore, extend and unify the jurisdiction of such a transition in the entire family of hyperbolic electronic fluids, while its precursor semimetal-to-metal QPT is exclusively observed in hyperbolic Dirac systems.

Model. The NN-TBM for spinless fermions on an underlying hyperbolic or Euclidean lattice in the presence

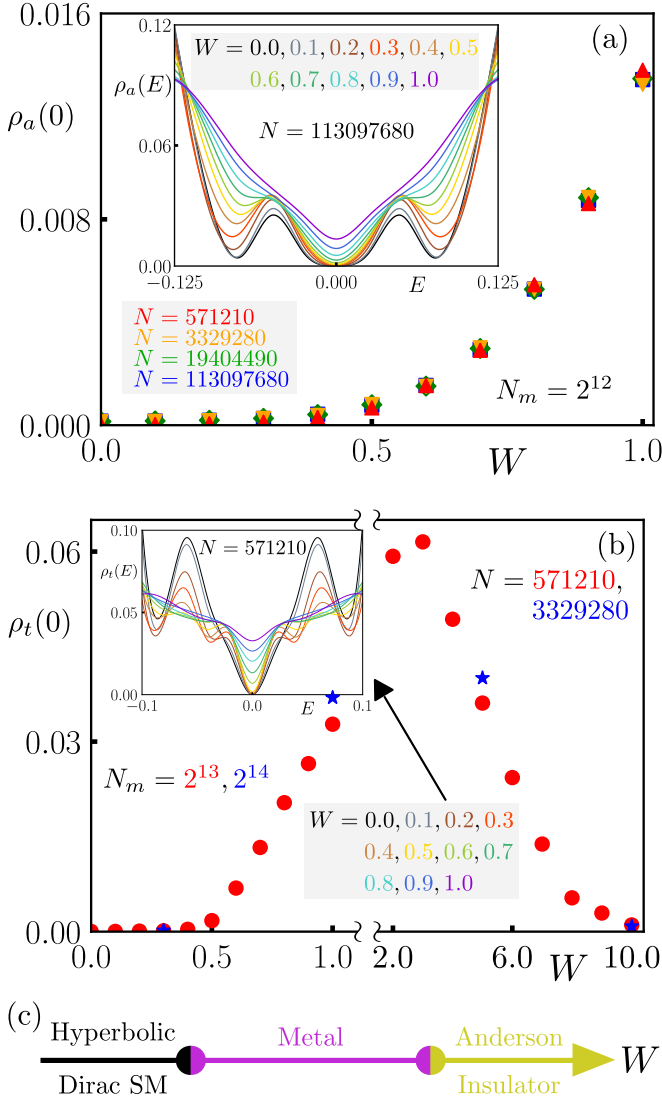


FIG. 1. (a) Average density of states (DOS) at zero energy $\rho_a(0)$ as a function of disorder strength (W). Inset shows $\rho_a(E)$ vs E (energy). (b) Typical DOS at zero energy $\rho_t(0)$, averaged over the system (see text), as a function of W . Inset shows $\rho_t(E)$ vs E . Here, N (N_m) denotes the number of sites (Chebyshev moments). (c) A schematic phase diagram of disordered hyperbolic Dirac semimetal (SM), where circles denote quantum critical points, separating the adjacent phases. All the results are for $\{10, 3\}$ lattices.

of random pointlike charge impurities reads as

$$H = -t \sum_{\langle i,j \rangle} c_i^\dagger c_j + \sum_i V(\mathbf{r}_i) c_i^\dagger c_i. \quad (1)$$

Here, c_i^\dagger (c_i) is the fermionic creation (annihilation) operator on the i th site, t is the real NN hopping amplitude (set to be unity), $\langle \dots \rangle$ restricts the summation within the NN sites, and on each site i located at \mathbf{r}_i a disorder potential $V(\mathbf{r}_i)$ is drawn randomly and independently from a box distribution $[-W/2, W/2]$, with real W denoting its

strength. Within the framework of the NN-TBM, lattices with even integer p manifest (microscopic or emergent) bipartite structure, which can be appreciated in the following way. We attach a sublattice label A or B to each site such that any pair of NN sites belong to complementary sublattices. Next, define an N -component spinor $\Psi^\top = (c_A, c_B)$, where c_A (c_B) is an $N/2$ -dimensional spinor constituted by the annihilation operators on the sites belonging to the A (B) sublattice and N is the total number of sites in the system. In this basis, the Hermitian matrix associated with the NN-TBM in the absence of disorder takes the form $\hat{h}_0 = \begin{pmatrix} \mathbf{0} & \mathbf{t} \\ \mathbf{t}^\top & \mathbf{0} \end{pmatrix}$, where $\mathbf{0}$ is an $N/2$ -dimensional null matrix, \mathbf{t} is an $N/2$ -dimensional real inter-sublattice hopping matrix, and \top represents transposition. Such an operator preserves the time reversal symmetry, generated by $\mathcal{T} = \mathbb{I}_N \mathcal{K}$, where \mathbb{I}_N is an N -dimensional identity matrix and \mathcal{K} is the complex conjugation, such that $[\hat{h}_0, \mathcal{T}] = 0$ with $\mathcal{T}^2 = +1$, which remains unaltered even in the presence of on-site charge impurities. Hence, the system belongs to the *orthogonal* class. The same operator \hat{h}_0 also preserves an antiunitary particle-hole symmetry, generated by $\mathcal{C} = \Sigma_z \mathcal{K}$, where $\Sigma_z = \text{diag.}(\mathbb{I}_{N/2}, -\mathbb{I}_{N/2})$ such that $\{\hat{h}_0, \mathcal{C}\} = 0$ and $\mathcal{C}^2 = +1$. The operator \hat{h}_0 also possesses a unitary particle-hole or chiral or sublattice symmetry, generated by $\mathcal{S} = \Sigma_z$ such that $\{\hat{h}_0, \mathcal{S}\} = 0$. Hence, the NN-TBM on *clean* bipartite hyperbolic and Euclidean lattices belongs to the chiral orthogonal or BDI class [21, 22]. Here, we exclusively focus on $\{10, 3\}$ and $\{6, 3\}$ lattices.

Systems. Throughout we impose open boundary conditions on $\{10, 3\}$ lattices to monitor the effects of its edges, encompassing a large fraction of the total number of sites. On honeycomb lattices numerical calculations are performed with periodic boundary conditions to eliminate the effects of zero energy topological modes on its zigzag edges. We characterize the system size by N or its total generation number (n_{tot}). The generation number (n) is defined in the following way. The central p gon constitutes the first generation ($n = 1$) and each successive layer of plaquettes constitutes its progressively next generation. The largest $\{10, 3\}$ system on which we compute average (typical) DOS contains $N > 10^8$ ($N > 10^5$). On honeycomb lattices, we only compute typical DOS, and the largest system contains $N > 10^6$.

Density of states. We employ the KPM to compute average and typical DOS. The disorder-averaged, denoted by $\langle \dots \rangle$, average DOS at energy E is defined as

$$\rho_a(E) = \left\langle \frac{1}{N} \sum_{j=1}^N \delta(E - E_j) \right\rangle. \quad (2)$$

Although $\rho_a(E)$ is a self-averaging quantity, we average it over 10 independent disorder realizations to minimize residual statistical errors. We typically compute 4096 Chebyshev moments (N_m) and take a trace over 12

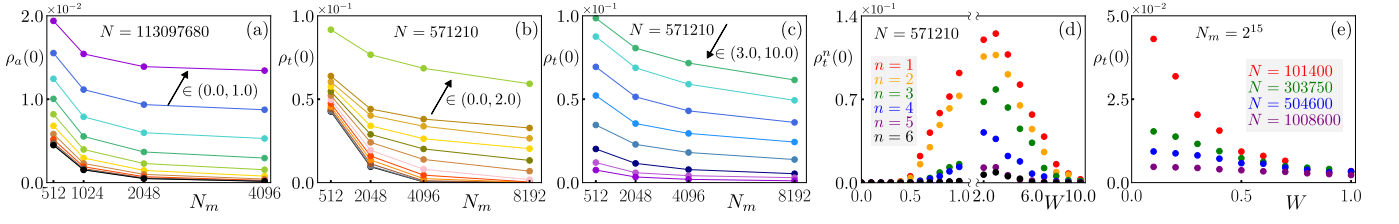


FIG. 2. (a) Variation of the average density of states (DOS) at zero energy $\rho_a(0)$ in a $\{10, 3\}$ system containing $N(> 10^8)$ sites (see legend) with N_m number of Chebyshev moments for disorder strengths ranging from 0.0 to 1.0 in steps of 0.1 in the direction of the arrow. (b) Same as (a), but for the typical DOS at zero energy $\rho_t(0)$, containing additional results for $W = 2.0$. (c) Same as (b), but for disorder strengths ranging from 3.0 to 10.0 in steps of 1.0 in the direction of the arrow. (d) Typical DOS at zero energy $\rho_t^n(0)$, computed only on the decagon belonging to the n th generation of a $\{10, 3\}$ lattice with a total of $n_{\text{tot}} = 6$ generations hosting N number of sites (see legend), where $1 \leq n \leq n_{\text{tot}}$. (e) Variation of $\rho_t(0)$ with W on honeycomb or $\{6, 3\}$ lattices with increasing system size or number of sites N therein (see legend) for a fixed $N_m = 2^{15}$.

unimodular random vectors while computing $\rho_a(E)$ [16]. The local DOS at the i th site at energy E is defined as

$$\rho_{\text{loc}}^i(E) = \sum_{j=1}^N |\langle E_j | i \rangle|^2 \delta(E - E_j), \quad (3)$$

where $|i\rangle$ is the site-localized Wannier wavefunction, and $|E_j\rangle$ is the eigenstate with energy E_j . The typical DOS over a p -gon from the n th generation is defined as

$$\rho_t^n(E) = \exp\left(\frac{1}{p} \sum_{i=1}^p \langle \ln \rho_{\text{loc}}^i(E) \rangle\right). \quad (4)$$

During the computation of $\rho_{\text{typ}}^n(E)$, we usually compute 8192 Chebyshev moments and average over 60 independent disorder realizations as it is not a self-averaging quantity. Computation of Chebyshev moments is always augmented by the Jackson kernel to minimize the Gibbs oscillations. We compute typical DOS in each generation of $\{10, 3\}$ lattices to scrutinize the role of the large number of boundary sites. We also compute the scaling of the *average* typical DOS, defined as $\rho_t(E) = \sum_{n=1}^{n_t} \rho_t^n(E) / n_{\text{tot}}$. On $\{6, 3\}$ lattices, $\rho_t(E) \equiv \rho_t^n(E)$, which is insensitive to the location of the hexagon.

Results and phase diagram. On a $\{10, 3\}$ lattice with $n_{\text{tot}} = 9$ yielding $N > 10^8$, $\rho_a(0)$ remains pinned to zero ($\leq 10^{-3}$) up to $W = 0.4$, beyond which it becomes finite for $N_m = 4096$. These outcomes are insensitive to the system size as long as $n_{\text{tot}} \geq 6$ or equivalently $N > 10^5$. See Fig. 1(a). We confirm the convergence of these results with respect to N_m ; see Fig. 2(a). In parallel we also track the scaling of $\rho_t(0)$ (averaged typical DOS at energy $E = 0$) with W , on a $\{10, 3\}$ lattice with $n_{\text{tot}} = 6$ or $N > 10^5$ for $N_m = 8192$, showing a qualitatively similar behavior as $\rho_a(0)$. Specifically, $\rho_t(0)$ remains pinned to zero ($\leq 10^{-3}$) up to $W = 0.4$, only beyond which $\rho_t(0)$ becomes finite, as shown in Fig. 1(b). The convergence of these findings with respect to the number of Chebyshev moments is shown in Fig. 2(b). Together, the scaling of $\rho_a(0)$ and $\rho_t(0)$ with W strongly suggests that the

Hyperbolic Dirac semimetal is a stable phase of matter up to a critical disorder strength of $W_{c,1} = 0.4 \pm 0.1$. And for $W > W_{c,1}$, the system becomes a stable diffusive metal, characterized by finite $\rho_a(0)$ and $\rho_t(0)$, which we track in tandem up to $W = 1.0$.

For $W > 1.0$, we only compute $\rho_t(0)$ and notice that $\rho_{\text{typ}}(0) \rightarrow 0$ around a critical value $W_{c,2} = 10.0 \pm 1.0$, marking the critical point associated with the Anderson metal-to-insulator QPT; see Fig. 1(b). The convergence of these results with respect to N_m is shown in Fig. 2(c). With these results in hand, we arrive at the global phase of 2D dirty hyperbolic Dirac fluids, schematically shown in Fig. 1(c). Our numerical findings show that such systems feature three distinct stable phases of matter, a disordered semimetal at sufficiently weak disorder, a diffusive metal at moderate disorder, and the Anderson insulator at sufficiently strong disorder. Two quantum critical points separate these three phases.

The imprints of the boundary, containing a large fraction of the total number of sites on a hyperbolic lattice with open boundary conditions, can be observed from the scaling of $\rho_t^n(0)$ with W , shown in Fig. 2(d) for a $\{10, 3\}$ lattice with $n_{\text{tot}} = 6$. We note that $\rho_t^n(0)$ qualitatively follows the trend of $\rho_t(0)$ for any n . Specifically, $\rho_t^n(0)$ remains pinned zero for sufficiently weak and strong disorder for any n . However, with increasing n , the generation-dependent critical disorder strength $W_{c,1}^n$, defined as the disorder where $\rho_t^n(0)$ first becomes finite, increases, whereas $W_{c,2}^n$ where $\rho_t^n(0)$ subsequently becomes zero decreases. Furthermore, with increasing n , the magnitude of $\rho_t^n(0)$ decreases in the metallic phase. These findings suggest that on disordered hyperbolic Dirac systems with open boundary conditions, the regime of stability of the semimetal and Anderson insulator (diffusive metal) increases (decreases) as we traverse from the bulk of the lattice toward its boundary. In other words, in terms of $\rho_t^n(0)$, there exist no *unique* values for $W_{c,1}$ and $W_{c,2}$. However, the value of $W_{c,1}$, obtained from the scaling of $\rho_t(0)$ matches well with the one from the scaling

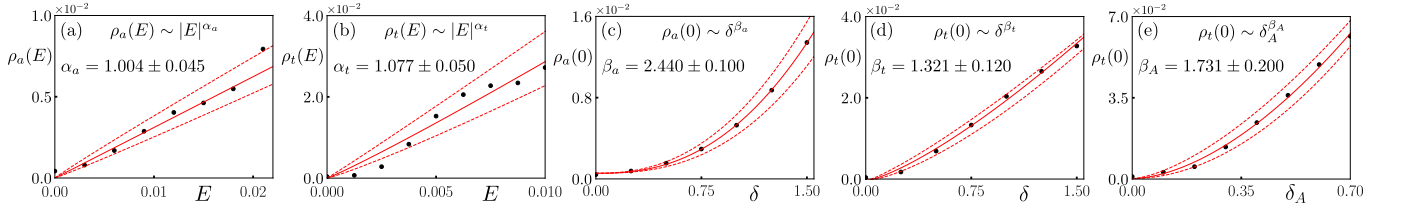


FIG. 3. Computation of density of states (DOS) exponents from the scaling of the (a) average (α_a) and (b) typical (α_t) DOS at finite energies (E) and order-parameter exponents from the scaling of the (c) average (β_a) and (d) typical (β_t) DOS at $E = 0$ near the semimetal-to-metal critical point at $W = W_{c,1}$, where W is disorder strength and $\delta = (W - W_{c,1})/W_{c,1}$. (e) Order-parameter exponent (β_A) near the Anderson critical point at $W = W_{c,2}$ from the scaling of typical DOS at zero energy with $\delta_A = (W_{c,2} - W)/W_{c,2}$. For (a) and (c) [(b), (d), and (e)], analyses were performed on $\{10, 3\}$ lattices with $n_{\text{tot}} = 9$ [$n_{\text{tot}} = 6$], containing more than 10^8 (10^5) sites. The scaling forms and values of the exponents are quoted in the legends.

of $\rho_a(0)$. For the Anderson transition, we take $W_{c,2}$ obtained from the scaling of $\rho_t(0)$ for the scaling analysis.

To attribute such peculiar outcomes in (chiral) orthogonal class Dirac semimetals [Fig. 1(c)] to its background negative spatial curvature, we compute $\rho_t(0)$ on honeycomb lattices with periodic boundary conditions in all directions. The results are shown in Fig. 2(e), depicting that $\rho_{\text{typ}}(0) \rightarrow 0$ for arbitrarily weak disorder as the system size approaches the thermodynamic limit $N \rightarrow \infty$ or $n_{\text{tot}} \rightarrow \infty$. These numerical findings are consistent with the standard wisdom that dirty orthogonal class systems always exist in the Anderson insulating phase [17].

An explanation. Presently, there exists no field theoretic explanation for the global phase diagram of disordered Hyperbolic Dirac systems, especially the existence of a stable dirty semimetal and its QPT into a metal. Such outcomes can possibly be explained in the following way. The (average) DOS for clean hyperbolic Dirac systems scales as $\rho_a(E) \sim E \tanh(E)$ in the absence of any external fields [23], which for small energies yields $\rho_a(E) \sim |E|^2$. See the inset of Fig. 1(a). We also note that as $E \rightarrow 0$, $\rho_t(E) \sim |E|^2$, as shown in the inset of Fig. 1(b), as in a stable semimetallic phase average and typical DOS follow each other. However, in small $\{10, 3\}$ lattices containing only a several thousand ($\sim 10^3 - 10^4$) sites (systems being effectively flat) $\rho(E) \sim |E|$ [2, 3], thereby unfolding the paramount importance of the underlying spatial curvature on the power-law scaling of the DOS, which only gets revealed in sufficiently large systems. These findings are in stark contrast with a recent proposal of a finite $\rho_a(0)$ in clean $\{10, 3\}$ lattices [24].

With such a scaling of the DOS, a qualitative explanation in favor of a stable dirty hyperbolic Dirac semimetal can now be put forward from the scaling of the quasiparticle lifetime (τ), obtained from the self-consistent Born approximation [25], leading to (for $\hbar = 1$)

$$W \int_0^{E_\Lambda} \frac{\rho_a(E)}{\tau^{-2} + E^2} dE = 1 \quad (5)$$

where E_Λ is an ultraviolet energy cutoff up to which $\rho_a(E) \sim |E|^2$ and we note that $1/\tau \sim \rho_a(0)$. The

integral shows a *linear* ultraviolet divergence, which can be regulated by defining a critical disorder $W_c = \int_0^{E_\Lambda} (\rho_a(E)/E^2) dE$. Then in terms of the reduced distance from the critical point at $W = W_c$, defined as $\delta = (W - W_c)/W_c$, we find $\tau^{-1} = (2/\pi) \delta$ (after taking $E_\Lambda \rightarrow \infty$). Thus quasiparticle lifetime becomes finite, indicating the onset of a diffusive metal with a finite $\rho_a(0)$, only when $\delta > 0$ or $W > W_c$. So far, we have used $W_c \equiv W_{c,1}$. By contrast, the stability of a metallic state and its transition to an Anderson insulator possibly results from the natural infrared cutoff (related to the radius of the hyperbolic space) for the probability of self-returning paths on a negatively curved space [20].

Critical exponents. Finally, we compute the *universal* critical exponents near two QPTs in dirty hyperbolic Dirac systems. Across the semimetal-to-metal QPT, we can define the DOS exponents α_a and α_t from the following scaling forms $\rho_a(E) \sim |E|^{\alpha_a}$ and $\rho_t(E) \sim |E|^{\alpha_t}$, respectively, yielding $\alpha_a = 1.004 \pm 0.045$ [Fig. 3(a)] and $\alpha_t = 1.077 \pm 0.050$ [Fig. 3(b)], which are sufficiently close to each other. The order parameter exponents across this transitions β_a and β_t are defined as $\rho_a \sim \delta^{\beta_a}$ and $\rho_t \sim \delta^{\beta_t}$, respectively, for $\delta > 0$ where $\delta = (W - W_{c,1})/W_{c,1}$, and we obtain $\beta_a = 2.440 \pm 0.100$ [Fig. 3(c)] and $\beta_t = 1.321 \pm 0.120$ [Fig. 3(d)]. The difference in the numerically obtained values of β_a and β_t is strongly suggestive of wavefunction multifractality across the semimetal-to-metal QPT [26]. The order-parameter exponent across the Anderson transition β_A , defined as $\rho_t(0) \sim \delta_A^{\beta_A}$ with $\delta_A = (W_{c,2} - W)/W_{c,2} > 0$, is found to be $\beta_A = 1.731 \pm 0.200$ [Fig. 3(e)].

Summary and discussions. To summarize, based on strong numerical evidence we argue that massless Dirac fermions living on a negatively curved space, resulting from the prototypical NN-TBM on 2D $\{10, 3\}$ hyperbolic lattices, are stable against sufficiently weak disorder. However, at moderate disorder the system undergoes a continuous QPT into a diffusive metallic phase, which ultimately encounters a transition into an Anderson insulator at even stronger disorder. As such systems

belong to the orthogonal class, these findings present concrete counterexamples to traditional wisdom, which, however, applies to 2D Euclidean systems such as dirty honeycomb lattices, where the fermionic degrees of freedom always exist in the Anderson localized phase. Thus, the background constant negative spatial curvature can safely be solely credited for the observed quantum peculiarities in dirty hyperbolic Dirac fluids. Even though we offer a qualitative explanation, particularly for the hyperbolic Dirac semimetal-to-metal QPT, its field theoretic justification is still lacking, which should motivate future works. As a final remark, we note that the global phase diagram of dirty 2D hyperbolic Dirac liquids closely resembles the one for vastly studied three-dimensional Euclidean disordered Dirac and Weyl systems [27–36]. However, the associated critical exponents are sufficiently distinct (namely, β_a , β_t , and β_A , but not α_a or α_t), suggesting that universality classes for the semimetal-to-metal QPT in these two systems are distinct and the spatial curvature plays a critical role in determining the universality classes of the QPTs in the former family of systems.

Acknowledgments. This work was supported by NSF CAREER Grant No. DMR-2238679 of B.R. B.R. is indebted to Vladimir Juričić for invaluable correspondences and critical comments on the manuscript.

-
- [1] N. W. Ashcroft and N. D. Mermin, *Solid State Physics* (Brooks Cole, Emeryville, CA, 1976).
 - [2] N. Gluscevic, A. Samanta, S. Manna, and B. Roy, Dynamic mass generation on two-dimensional electronic hyperbolic lattices, *Phys. Rev. B* **111**, L121108 (2025).
 - [3] C. A. Leong and B. Roy, Non-Hermitian catalysis of density-wave orders on Euclidean and hyperbolic lattices, [arXiv:2501.18591](#).
 - [4] A. Comtet and P. J. Houston, Effective action on the hyperbolic plane in a constant external field, *J. Math. Phys.* **26**, 185 (1985).
 - [5] J. Maciejko and S. Rayan, Hyperbolic band theory, *Sci. Adv.* **7**, eabe9170 (2021).
 - [6] I. Boettcher, A. V. Gorshkov, A. J. Kollár, J. Maciejko, S. Rayan, and R. Thomale, Crystallography of hyperbolic lattices, *Phys. Rev. B* **105**, 125118 (2022).
 - [7] J. Maciejko and S. Rayan, Automorphic Bloch theorems for hyperbolic lattices, *Proc. Natl. Acad. Sci. USA* **119**, e2116869119 (2022).
 - [8] T. Tummuru, A. Chen, P. M. Lenggenhager, T. Neupert, J. Maciejko, and T. Bzdušek, Hyperbolic Non-Abelian Semimetal, *Phys. Rev. Lett.* **132**, 206601 (2024).
 - [9] A. Chen, J. Maciejko, and I. Boettcher, Anderson Localization Transition in Disordered Hyperbolic Lattices, *Phys. Rev. Lett.* **133**, 066101 (2024).
 - [10] S. Dey, A. Chen, P. Basteiro, A. Fritzsche, M. Greiter, M. Kaminski, P. M. Lenggenhager, R. Meyer, R. Sorbello, A. Stegmaier, R. Thomale, J. Erdmenger, and I. Boettcher, Simulating Holographic Conformal Field Theories on Hyperbolic Lattices, *Phys. Rev. Lett.* **133**, 061603 (2024).
 - [11] B. Roy, Magnetic catalysis in weakly interacting hyperbolic Dirac materials, *Phys. Rev. B* **110**, 245117 (2024).
 - [12] A. Götz, G. Rein, J. C. Inácio, and F. F. Assaad, Hubbard and Heisenberg models on hyperbolic lattices: Metal-insulator transitions, global antiferromagnetism, and enhanced boundary fluctuations, *Phys. Rev. B* **110**, 235105 (2024).
 - [13] A. Djordjević, M. Dimitrijević Ćirić, and V. Juričić, Symmetry-based theory of Dirac fermions on two-dimensional hyperbolic crystals: Coupling to the spin connection, [arXiv:2507.08276](#).
 - [14] J. C. Slonczewski and P. R. Weiss, Band Structure of Graphite, *Phys. Rev.* **109**, 272 (1958).
 - [15] G. W. Semenoff, Condensed-Matter Simulation of a Three-Dimensional Anomaly, *Phys. Rev. Lett.* **53**, 2449 (1984).
 - [16] A. Weiße, G. Wellein, A. Alvermann, and H. Fehske, The kernel polynomial method, *Rev. Mod. Phys.* **78**, 275 (2006).
 - [17] E. Abrahams, P. W. Anderson, D. C. Licciardello, and T. V. Ramakrishnan, Scaling theory of localization: Absence of quantum diffusion in two dimensions, *Phys. Rev. Lett.* **42**, 673 (1979).
 - [18] M. P. A. Fisher and E. Fradkin, Localization in a magnetic field: Tight binding model with one-half of a flux quantum per plaquette, *Nucl. Phys. B* **251**, 457 (1985).
 - [19] A. Chen, J. Maciejko, and I. Boettcher, Anderson Localization Transition in Disordered Hyperbolic Lattices, *Phys. Rev. Lett.* **133**, 066101 (2024).
 - [20] J. B. Curtis, P. Narang, and V. Galitski, Absence of Weak Localization on Negative Curvature Surfaces, *Phys. Rev. Lett.* **134**, 076301 (2025).
 - [21] A. Altland and M. R. Zirnbauer, Nonstandard symmetry classes in mesoscopic normal-superconducting hybrid structures, *Phys. Rev. B* **55**, 1142 (1997).
 - [22] S. Ryu, A. P. Schnyder, A. Furusaki and A. W. W. Ludwig, Topological insulators and superconductors: tenfold way and dimensional hierarchy, *New J. Phys.* **12**, 065010 (2010).
 - [23] A. Comtet, On the Landau levels on the hyperbolic plane, *Ann. Phys. (N.Y.)* **173**, 185 (1987).
 - [24] R. Mosseri and J. Vidal, Density of states of tight-binding models in the hyperbolic plane, *Phys. Rev. B* **108**, 035154 (2023).
 - [25] P. Sheng, *Introduction to Wave Scattering, Localization, and Mesoscopic Phenomena* (Springer, Berlin, 2006).
 - [26] F. Evers and A. D. Mirlin, Anderson transitions, *Rev. Mod. Phys.* **80**, 1355 (2008).
 - [27] E. Fradkin, Critical behavior of disordered degenerate semiconductors. II. Spectrum and transport properties in mean-field theory, *Phys. Rev. B* **33**, 3263 (1986).
 - [28] Y. Ominato and M. Koshino, Quantum transport in a three-dimensional Weyl electron system, *Phys. Rev. B* **89**, 054202 (2014).
 - [29] P. Goswami and S. Chakravarty, Quantum Criticality between Topological and Band Insulators in 3 + 1 Dimensions, *Phys. Rev. Lett.* **107**, 196803 (2011).
 - [30] K. Kobayashi, T. Ohtsuki, K.-I. Imura, and I. F. Herbut, Density of States Scaling at the Semimetal to Metal Transition in Three Dimensional Topological Insulators, *Phys. Rev. Lett.* **112**, 016402 (2014).
 - [31] B. Sbierski, G. Pohl, E. J. Bergholtz, and P. W. Brouwer, Quantum Transport of Disordered Weyl Semimetals at the Nodal Point, *Phys. Rev. Lett.* **113**, 026602 (2014).

- [32] S. V. Syzranov, L. Radzihovsky, and V. Gurarie, Critical Transport in Weakly Disordered Semiconductors and Semimetals, [Phys. Rev. Lett. **114**, 166601 \(2015\)](#).
- [33] J. H. Pixley, P. Goswami, and S. Das Sarma, Anderson Localization and the Quantum Phase Diagram of Three Dimensional Disordered Dirac Semimetals, [Phys. Rev. Lett. **115**, 076601 \(2015\)](#).
- [34] S. Bera, J. D. Sau, and B. Roy, Dirty Weyl semimetals: Stability, phase transition, and quantum criticality, [Phys. Rev. B **93**, 201302\(R\) \(2016\)](#).
- [35] B. Roy, R.-J. Slager, and V. Juričić, Global Phase Diagram of a Dirty Weyl Liquid and Emergent Superuniversality, [Phys. Rev. X **8**, 031076 \(2018\)](#).
- [36] I. Balog, D. Carpentier, and A. A. Fedorenko, Disorder-Driven Quantum Transition in Relativistic Semimetals: Functional Renormalization via the Porous Medium Equation, [Phys. Rev. Lett. **121**, 166402 \(2018\)](#).